

Plasma Source Test and Simulation Results for the Underdense Plasma Lens Experiment at the UCLA Neptune Laboratory

H. Suk, C. E. Clayton, C. Joshi, T. C. Katsouleas, P. Muggli, R. Narang, C. Pellegrini, and J. B. Rosenzweig

Abstract—The planned plasma lens experiment at the UCLA Neptune Laboratory is described. In the experiment, electron beams with an energy of 16 MeV, a charge of 4 nC, and a pulse duration of 30 ps [full-width at half-maximum (FWHM)] are designed to be produced from the 1.625-cell photoinjector radio-frequency gun ($f = 2.856$ GHz) and PWT linac in the Neptune. The generated beams are passed through a thin underdense argon plasma with a density of low 10^{12} cm $^{-3}$ range and a thickness of a few centimeters. For this experiment, a LaB $_6$ -based discharge plasma source was developed and tested. In this paper, the overview of the planned plasma lens experiment and the test results of the plasma source for various conditions are presented. In addition, computer simulations with a 2-1/2 dimensional particle-in-cell code (MAGIC) were performed and the simulation results are shown.

Index Terms—Discharge plasma, electron beam, photoinjector, plasma lens.

I. INTRODUCTION

FOCUSING charged particle beams with plasmas has been studied extensively both theoretically and experimentally. Although it has a rather long history [1], [2], new applications and methods are still developed and studied. In recent years, for example, plasma-based lenses are actively studied for potential applications to final focusing of next-generation $e^- + e^+$ linear colliders because high-density plasmas can provide an extremely strong focusing force [3]–[5]. In addition, plasma wake-field acceleration [6]–[9] is studied in connection with plasma lenses.

Basically, plasma lenses for electron beams can be divided into two types, depending on relative plasma density to beam density: overdense and underdense plasma lenses. In the overdense regime, the plasma density n_p is larger than the electron beam density n_b . In this case, the beam charge is almost completely neutralized, but the current is partially

neutralized because of a rather large skin depth compared to the beam size. Hence, the focusing force is dependent on the transverse beam density profile. Since transverse beam densities are generally nonuniform, the transverse focusing force is nonlinear. Therefore, spherical aberrations are inevitable in the overdense plasma lenses. In the underdense regime ($n_p < n_b$), however, when a beam propagates in a plasma almost all plasma electrons are ejected from the electron beam cross-section due to a strong space-charge force of the beam. Background ions are much heavier than electrons, and the ion-plasma oscillation period is much longer than the beam pulse duration. In this case, the background ions are almost stationary. As a result, a nearly uniform ion channel is formed and this ion channel gives a radially linear focusing force to the beam. This is one of the major advantages of underdense plasma lenses over overdense plasma lenses.

As mentioned above, extensive theoretical and experimental works have been previously performed in the area of plasma focusing. However, the majority of the previous efforts were concentrated on overdense plasma lenses [10], [11]. Although some simulation and conceptual studies [4], [12], [13] have been done in the underdense plasma regime, little experimental work has been performed. At the Argonne Wakefield Accelerator Facility (AWA), experiments in the underdense plasma regime were done in association with plasma wake-field accelerations [14]. At AWA, they observed a nearly equilibrium transport of the beam body over many depths of focus (β). For useful plasma lenses, however, the plasma should be thin and strong so as to focus the beam well below its initial size. Another experiment is under way at SLAC (E-150). They use a gas jet and laser for high-density ($>10^{16}$ cm $^{-3}$) plasma generation. For this experiment, a very high energy beam (30 GeV) is used.

At the UCLA Neptune Laboratory, we have an ongoing plasma-lens experiment in thin underdense regime. Beam and plasma parameters are very different from the E-150 experiment at SLAC. For the experiment at UCLA, we developed and tested a discharge-based argon plasma source [15]. In this paper, the ongoing underdense plasma lens experiment is introduced, and the plasma source test results for the experiment are presented in Section II. In addition, simulations with the MAGIC PIC code [16] (2-1/2 dimensional fully electromagnetic, relativistic particle-in-cell code) have been performed to predict beam-plasma interaction phenomena and the results are presented in Section III. The summary is given in Section IV.

Manuscript received May 3, 1999; revised September 22, 1999. This work was supported by the U.S. Department of Energy under Grant DE-FG03-92ER40693 and by the National Science Foundation under Grant ECS9617089.

H. Suk, C. Pellegrini, and J. B. Rosenzweig are with the Department of Physics and Astronomy, University of California, Los Angeles, CA 90095 USA.

C. E. Clayton, C. Joshi, P. Muggli, and R. Narang are with the Department of Electrical Engineering, University of California, Los Angeles, CA 90095 USA.

T. C. Katsouleas is with the Department of Electrical Engineering and Quantum Electronics, University of Southern California, Los Angeles, CA 90089 USA.

Publisher Item Identifier S 0093-3813(00)01132-2.

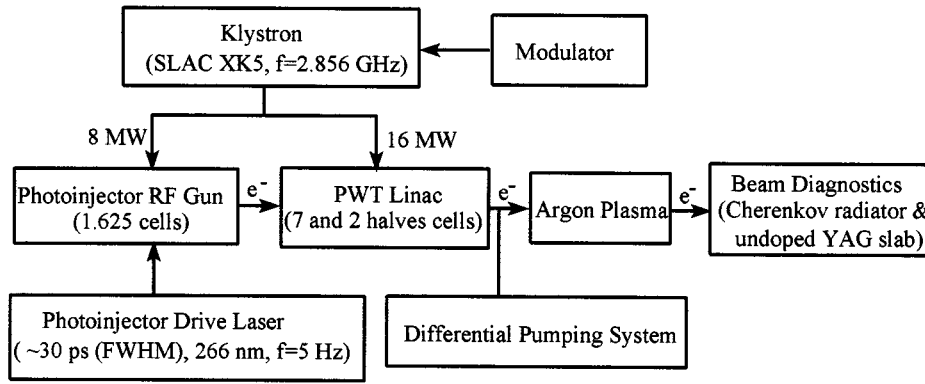


Fig. 1. Block diagram of the experimental facility.

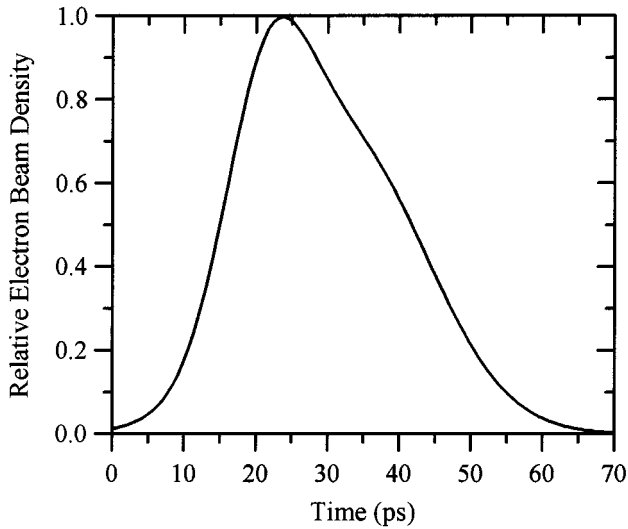


Fig. 2. Longitudinal beam density profile for the experiment.

II. PLANNED EXPERIMENT FOR A THIN UNDERDENSE PLASMA LENS AND TEST RESULTS OF THE PLASMA SOURCE

A. Overview of the Experiment and Design Parameters

For the underdense plasma lens experiment, the Neptune beamline [17] and the argon discharge plasma source are used. Fig. 1 shows a block diagram for the experiment. As shown, the experimental facility consists of the photocathode radio-frequency (RF) gun (1.625 cells), PWT linac (7 and 2 half-cells), Klystron (SLAC XK5, $f = 2.856$ GHz), photocathode drive laser ($\lambda = 266$ nm), plasma source, diagnostic tools, etc. In this experiment, long pulse electron beams will be used, which are defined here as beams such that the beam duration T_b is longer than the electron-plasma oscillation period ω_p^{-1} . Fig. 2 shows the approximate electron beam profile [full-width at half-maximum (FWHM) pulse duration $\simeq 30$ ps], which was used in the previous overdense plasma lens experiment at UCLA, and a similar beam profile will be used in the new underdense plasma lens experiment. In this scheme, the front part of the beam is used to produce a uniform ion channel, and the remaining part of the beam (rear part) is focused due to the ion channel made by the front part of the beam. For this purpose, the front part of the beam should last for longer than

the plasma oscillation period ω_p^{-1} . To generate this kind of long pulse electron beams, long laser pulses are used, unlike in other experiments at the Neptune Laboratory. The long laser pulses can be generated by bypassing the frequency chirping optical fiber and the pulse compressing gratings in the present photocathode drive laser system [18]. In other words, $1.064\text{-}\mu\text{m}$ mode-locked Nd:YAG laser beams ($\sim 80\text{-ps}$ FWHM) from Antares are directly injected into the Nd:glass regenerative amplifier, and then the laser beams are sent to the two frequency-doubling crystals (BBO's) for frequency quadrupling. In this process, the pulse length is shortened by the nonlinear crystals because conversion efficiency in the crystals is approximately proportional to the square of the input laser intensity. Hence, the shortened ultraviolet (266 nm) light is eventually injected into the copper photocathode RF gun for photoelectron generation. The electron beams are accelerated to about 4.5 MeV by the RF gun, and they are further accelerated to about 16 MeV by the PWT linac. The high energy electron beams are then injected into the plasma chamber for focusing. Since pressure in the plasma chamber is in the several mtorr range and the RF gun requires high vacuum, a differential pumping system is placed between the beamline and plasma chamber to separate them.

Experimental design parameters for the beam and plasma are summarized in Table I. As shown in the table, long and high-charge electron beams with 30-ps duration (FWHM) and 4 nC are injected into the argon plasma with a density of $n_p \sim n_b/2$ (underdense) and a thickness of about 2 cm. In this case, it is estimated that the focal length f is about 7 cm and the beam size is reduced by a factor of about 0.14. The focal length is larger than the plasma thickness so that this plasma is a thin plasma lens. More detailed analysis and comparison with simulation results are presented in Section III.

The focused beams are analyzed with diagnostic tools. For taking time-integrated beam images, a charge-coupled-device camera and an undoped YAG slab with a thickness of 0.5 mm are used. The YAG slab is installed downstream of the plasma and can move longitudinally along the beam direction. Hence, transverse beam profile measurements at different positions yield information about dynamical plasma focusing. In addition to the YAG slab, a Cherenkov radiator and a streak camera with a few picoseconds resolution are used for time-resolved measurement of the beams. The Cherenkov radiator is also movable along the

TABLE I
DESIGN PARAMETERS FOR THE PLASMA LENS EXPERIMENT

electron beam energy $E = 16$ MeV
charge per bunch $Q = 4$ nC
beam duration (FWHM) $T_b = 30$ ps
normalized emittance $\epsilon_n = 10$ mm-mrad
beam radius at the plasma entrance $\sigma_0 = 400$ μm (transverse beam density $\propto e^{-r^2/2\sigma_0^2}$)
beam density $n_b = 2.6 \times 10^{12}$ cm^{-3}
plasma density $n_p \sim n_b/2$
plasma thickness ~ 2 cm

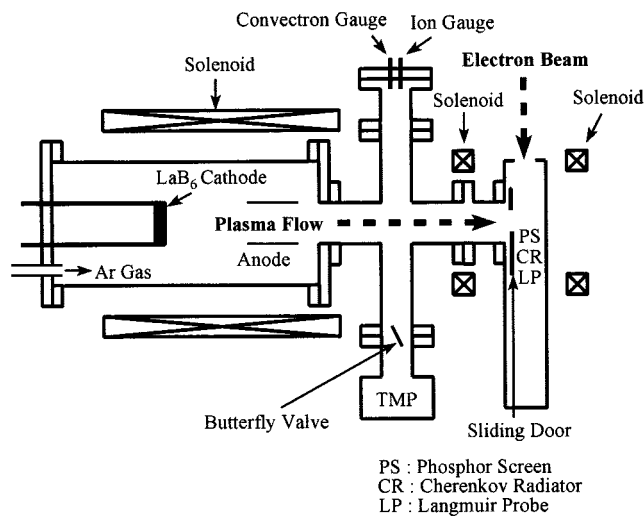


Fig. 3. Schematic of the plasma source.

beam path so that it can provide longitudinal dynamics information. The experimental results will be compared with computer simulations for further analysis.

B. Test Results of the Underdense Plasma Source

For experiments on the thin underdense plasma lens, an argon discharge plasma source was developed and tested for various conditions. Fig. 3 shows a schematic of the plasma source. The cathode is made of a LaB₆ disk with a diameter of 7 cm and is heated up to over $T_c = 1300$ °C. The anode consists of a hollow tantalum, and a rectangular pulse voltage of up to 110 V is applied between the anode and the cathode for several milliseconds. Since the chamber is filled with an argon gas in several mtorr range during operation, an electric discharge occurs between the anode and the cathode so that an argon plasma is generated. This plasma flows through the hollow anode and arrives at the beam-plasma interaction chamber with the help of a guiding magnetic field. The guiding magnetic field of 50–70 Gauss is generated by the three solenoids shown in Fig. 3. The beam-plasma interaction chamber has a sliding door at the entrance, so the plasma thickness can be adjusted with the sliding

door gap. An electron beam is designed to pass the plasma transversely, and a plasma density profile along the beam path is measured with an axially movable Langmuir probe in the chamber. Plasma density in the interaction chamber depends on various parameters such as cathode temperature, pressure, discharge voltage, magnetic field, and sliding door gap. Hence, these parameters were adjusted one by one to find the optimum condition for the experiment.

Measurements of the discharge current I_d versus the discharge voltage V_d for different cathode temperatures and argon gas pressures are shown in Fig. 4(a) and (b). As shown in the figures, I_d generally increases as V_d and pressure P increase, but dependence of I_d on P is weak. Instead, it is shown that I_d is strongly dependent on T_c . For example, a 4% increase in T_c leads to a 50% increase in I_d for $V_d = 100$ V and $P = 2$ mtorr. It means that I_d is dominated by T_c . It was also observed that for a higher cathode temperature and low pressure range, arcing was noticeably reduced. In the case of arcing, I_d was large (> 200 A), but a plasma density in the beam-plasma interaction chamber was observed very small. Hence, arcing should be avoided.

Fig. 5 shows the plasma density and temperature measurement result in the beam-plasma interaction chamber. It was obtained when the cathode temperature was 1330 °C and the sliding door gap was 2.5 cm. Fig. 5(a) shows that plasma density increases for higher discharge voltages. It also shows that for a fixed discharge voltage and magnetic field, a plasma density has a peak around 2 mtorr, and then it decreases as pressure increases further. This can be qualitatively explained as follows: a generated plasma density in the discharge region will be approximately linear to pressure in a low pressure regime, but it rapidly approaches saturation as the pressure is further increased (see Fig. 4). On the other hand, diffusion loss during transport from the discharge region to the measurement region is proportional to pressure. As a result, the plasma density at the measurement spot has a peaked curve.

The plasma density measurement indicates that the plasma is weakly ionized because the fraction of ionization is in the several percent range (less than 10%). If the fraction of ionization is too low and the effect of neutral particle collisions with the

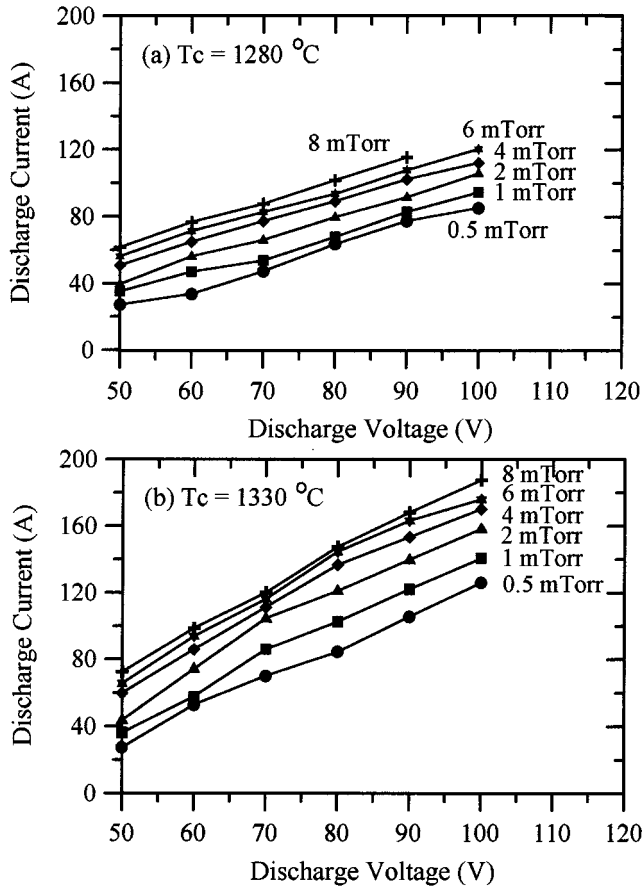


Fig. 4. Discharge current versus voltage for (a) $T_c = 1280$ °C and (b) $T_c = 1330$ °C.

high-energy electron beams is significant, it will be problematic. However, a mean free path in typical experimental conditions presented here is estimated to be much larger than the plasma size along the beam path. Therefore, collisional effects of high-energy electron beams with neutral particles are negligible.

Plasma transport from the discharge region to the measurement region is affected by the confining magnetic field. Since argon ions have a much larger Larmor radius than electrons, diffusion of weakly ionized argon plasma in a magnetic field is dominated by ions. Diffusion coefficient of a plasma across a magnetic field is approximately given by [19] $D_{\perp} = D(r_L/\lambda_m)^2 \propto B^{-2}$, where D is a diffusion coefficient when a magnetic field is absent, r_L is the Larmor radius, and λ_m is the mean free path. Therefore, plasma loss can be greatly suppressed by increasing the magnetic field. This was observed during plasma density measurements. In other words, a plasma density in the measurement region was shown to increase significantly as a magnetic field is increased. However, the magnetic field strength has an upper limit to use the Langmuir probe for plasma diagnostics, i.e., r_L should be larger than the Langmuir probe tip size. Furthermore, if the magnetic field is too strong, it will give too much transverse momentum to the incoming high energy electron beam, which leads to a significant beam path deflection. Hence, the magnetic field was adjusted within these requirements for best plasma

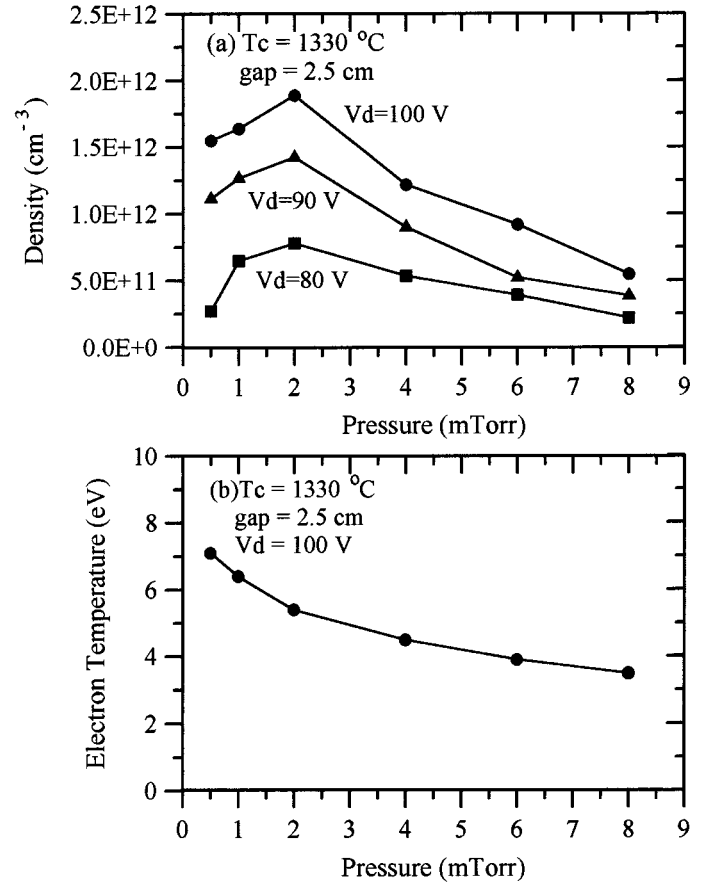


Fig. 5. Plasma density and temperature versus pressure for $T_c = 1330$ °C and a sliding door gap of 2.5 cm.

transport. In addition to plasma density, plasma temperature was also measured. An example for a discharge voltage of 100 V is shown in Fig. 5(b). As shown, the temperature is in the several eV range and decreases as pressure increases.

Longitudinal plasma density profile was measured by moving the Langmuir probe along the electron beam path. Two cases are shown in Fig. 6(a) and (b). Fig. 6(a) was obtained when the sliding door gap was 1.5 cm and the discharge voltage was 100 V. The density profile has a peak of 1.6×10^{12} cm $^{-3}$. To have a thinner plasma, the door gap was reduced to 1 cm and the plasma density was measured again. The result is shown in Fig. 6(b). As shown, the plasma thickness is smaller than in Fig. 6(a), and the peak plasma density (1.1×10^{12} cm $^{-3}$) is also reduced even though the discharge voltage is increased from 100 to 110 V. Here, it is needed to define an effective plasma length. Plasma focusing force in the underdense regime is proportional to plasma density so that it is appropriate to define the effective plasma thickness ℓ_p by

$$\ell_p = \frac{\int n_p(z)}{n_{p,0}} \quad (1)$$

where:

- $n_p(z)$ density profile function along the longitudinal direction;
- $n_{p,0}$ peak plasma density.

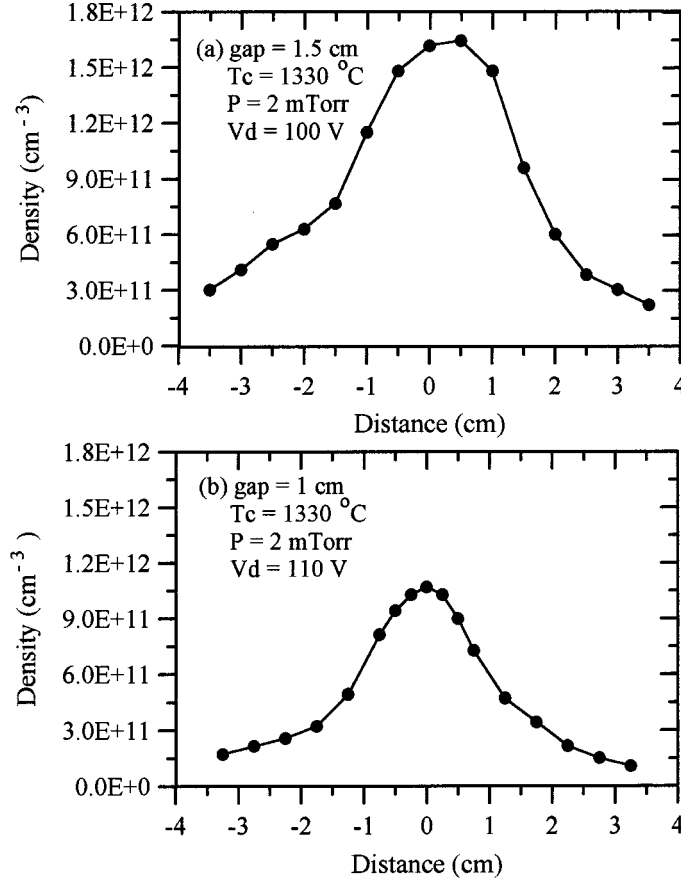


Fig. 6. Longitudinal plasma density profiles along the beam path for $T_c = 1330$ °C and $P = 2$ mtorr. (a) Sliding door gap = 1.5 cm, $V_d = 100$ V and (b) sliding door gap = 1 cm, $V_d = 110$ V.

According to this definition, the effective plasma thickness in Fig. 6(b) is 2.9 cm. Hence, the plasma parameters in Fig. 6(b) are more or less close to the design parameters for experiments.

III. SIMULATION RESULTS AND DISCUSSIONS

To predict experimental results, the 2-1/2 dimensional particle-in-cell code MAGIC was used for simulations. For the simulations, beam parameters in Table I and Fig. 2 are used, and the plasma is assumed to have the longitudinal density profile of $n_p(z) = n_{p,0} e^{-(z-z_1)^2/2\sigma_p^2}$, where $n_{p,0}$, z_1 , and σ_p are given by 1.1×10^{12} cm⁻³, 2.5 cm, and 0.9 cm, respectively. In this simulation, an electron beam is generated from the cathode at the position of 0 cm and propagates through the plasma. The temporal beam profile in Fig. 2 indicates that it takes about 24 ps to reach the maximum, which is longer than ω_p^{-1} . Therefore, plasma electrons will be almost adiabatically expelled from the beam path. Fig. 7 shows the dynamical focusing process of the beam electrons in this case. When the beam propagates through the plasma, the plasma takes a finite response time of $\omega_p^{-1} = 17$ ps. Therefore, the head part of the beam is not focused and, instead, the head part expands gradually because of beam emittance. This phenomenon is observed in Fig. 7. After a while ($\sim 2\omega_p$), however, plasma electrons are ejected from the beam path and the beam starts being focused, as shown in the figure.

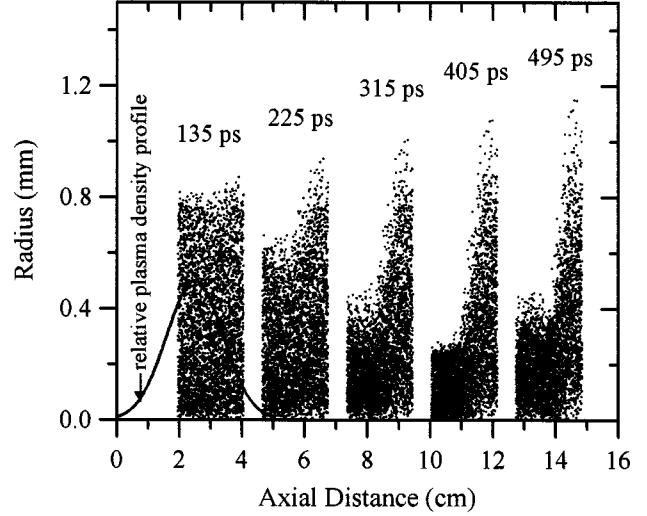


Fig. 7. Electron beam trajectory along the axial distance. In this simulation, the plasma slab and beam are assumed to have the parameters given by (2) and Table I.

Close investigation indicates that the plasma lens has a focus around $z = 11.5$ cm, i.e., the focal length f is about 9.0 cm in this case. Beyond the focal point, the beam starts expanding mainly because of the diverging emittance effect.

The focal length obtained from the simulation can be compared with the analytical formula for a thin plasma lens, based on the impulse focusing approximation [4]

$$f = 2\gamma c^2 / L_p \omega_p^2 \quad (2)$$

where

- γ Lorentz energy factor;
- c light speed;
- L_p plasma thickness.

It should be noted that the plasma thickness L_p is not equal to the effective plasma thickness ℓ_p , which was defined by (1). Since it takes a finite plasma response time of about ω_p^{-1} until the plasma acts as a focusing lens, it will be more accurate to define the plasma thickness L_p by

$$L_p = \ell_p - c\omega_p^{-1}. \quad (3)$$

In this simulation case, ℓ_p is calculated to be $\sqrt{2\pi}\sigma_p$, which is 2.25 cm, and $c\omega_p^{-1}$ is 0.51 cm. Hence, the plasma thickness L_p is 1.74 cm, and substitution of this into (2) leads to $f = 9.2$ cm, which is close to the simulation result. Therefore, the plasma lens can be called *thin* in the sense that its thickness is less than the focal length f . For the given beam and plasma parameters, the plasma is thin enough to avoid a beam emittance growth due to beam-plasma collisions because the plasma thickness is significantly smaller than $\lambda_\beta/4$. Here, λ_β is the betatron oscillation wavelength given by $\lambda_\beta = (2\pi\gamma/r_e n_p)^{1/2}$, where r_e is the classical electron radius.

As mentioned above, the plasma focusing force changes dynamically as time goes on. To investigate this phenomenon, the plasma focusing force at the center of the plasma slab ($z = 2.5$ cm) is obtained from the simulations for $\tau = \omega_p^{-1}$, $2\omega_p^{-1}$, and

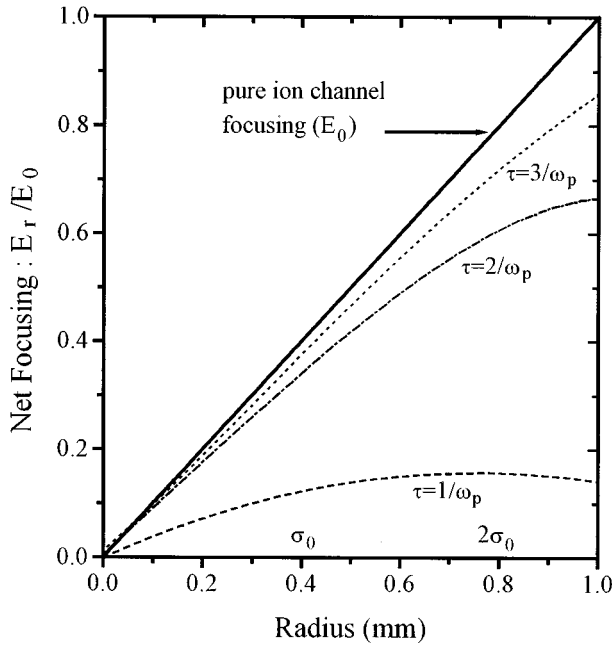


Fig. 8. Net focusing force versus radius at the plasma center ($z = 2.5$ cm). The solid line represents a focusing force for an electron-free pure ion channel, and dotted lines denote focusing forces at $\tau = \omega_p^{-1}$, $2\omega_p^{-1}$, and $3\omega_p^{-1}$, respectively.

$3\omega_p^{-1}$, respectively. Here, τ is defined by $\tau = t - z/v_b$. The result is shown in Fig. 8. In the figure, the solid line indicates the pure ion channel focusing given by $E_0 = n_{p,0}er/2\epsilon_0$, where:

- $n_{p,0}$ plasma density;
- e electron charge;
- r radial distance;
- ϵ_0 permittivity of free space.

The figure implies that plasma electrons are dynamically removed from inner radius to outer radius as time goes on. Roughly speaking, the majority of the plasma electrons are ejected from the beam path by $\tau = 2\omega_p^{-1}$ because 85% of the plasma electrons within $r = \sigma_0$ (0.4 mm) are removed by that time, and the focusing force is relatively linear up to $r = 2\sigma_0$. After $\tau = 3\omega_p^{-1}$, 93% of the plasma electrons within $r = \sigma_0$ are ejected, and the focusing force approaches the pure ion channel focusing more closely. Eventually almost all of the plasma electrons are expelled out far away from the beam path because the condition $k_p\sigma_0 \gg 1$ is satisfied. Here, the parameter k_p is defined by $k_p = \omega_p/c$. At other longitudinal positions in the plasma (i.e., $z \neq 2.5$ cm), however, the plasma density is lower than $n_{p,0}$ so that it will take a longer time for plasma electron ejection.

Nonlinear transverse focusing in Fig. 8 will change a current density profile downstream. To check this question, beam current densities were obtained at the focus position from the simulations. Fig. 9 shows electron beam current densities near the cathode ($z = 2$ mm) and at the focus ($z = 11.5$ cm) for comparison. It is observed that at the focus the beam size (FWHM) is reduced by a factor of 0.38 and 0.21 for $\tau = 2\omega_p^{-1}$ and $\tau = 3\omega_p^{-1}$, respectively. As assumed initially, the current density near the cathode is very close to Gaussian, while at the focus the density profile evolves to a non-Gaussian profile, i.e., the density profile

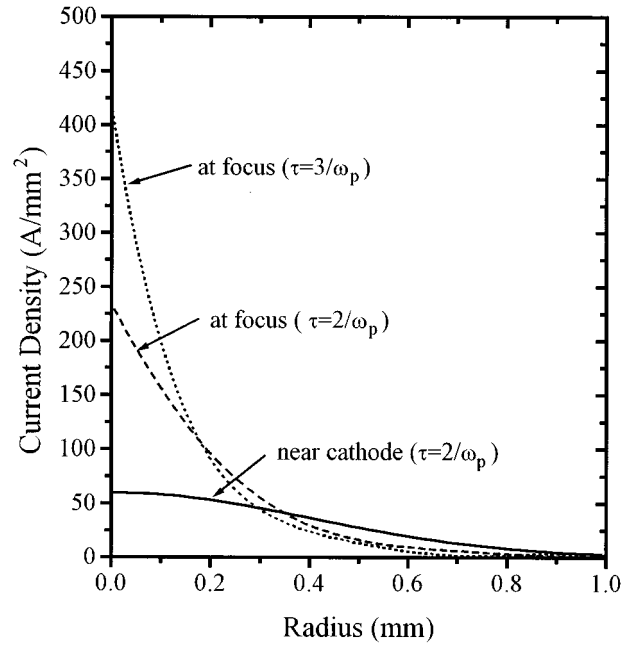


Fig. 9. Current density profiles near the cathode and at the focus.

is almost linear toward the beam axis. This kind of density profile deformation is believed to be caused by the highly dynamical and nonlinear plasma focusing, which persists until $3\omega_p^{-1}$. When the plasma gives a focusing force to the beam, the beam particles oscillate transversely at the beam plasma oscillation frequency of $\omega_b = (n_b e^2 / \gamma^3 m \epsilon_0)^{1/2}$. In the above example, the beam plasma oscillation wavelength ($2\pi c / \omega_b$) is calculated to be much longer than the focal length f so that the beam does not reach a thermal equilibrium until it propagates over the focal length f . In this kind of external-focusing-dominated situation, the density deformation will be directly affected by the nonlinear plasma focusing. However, it should be noted that the nonlinear focusing in this simulation is caused by the relatively short beams (beam pulse duration is approximately only a few ω_p^{-1}), which are available for the experiment. Hence, the nonlinearity in plasma focusing can be reduced if longer beams are used. Another way for reducing the nonlinearity is to increase the plasma density so that the plasma response time is reduced. In this case, the beam density should also be increased to maintain the underdense condition.

When an electron beam bunch propagates in the plasma, it will excite a longitudinal plasma wake field. Fig. 10 shows a graph of the longitudinal momentum P_z versus axial distance. In the figure, a longitudinal wake-field effect is evidently observed, i.e., during propagation in the plasma the electrons in the tail part of the beam bunch are accelerated and the electrons in the central part of the beam bunch are decelerated. The energy gain of the tail electrons is $\Delta E_{b+}/E_b = 0.2\%$ and energy loss of the central part electrons is $\Delta E_{b-}/E_b = 0.4\%$. Here, E_b , ΔE_{b+} , and ΔE_{b-} are the initial beam energy (16 MeV), gained energy of the tail part, and lost energy of the central part, respectively. Acceleration gradient of the wake field can be obtained from the figure, and it is approximately given by $E_z \sim 1$ MeV/m in the plasma. In addition, the transformer ratio of the wake field acceleration, defined by $R = \Delta E_{b+}/E_b$, is calculated as 0.5

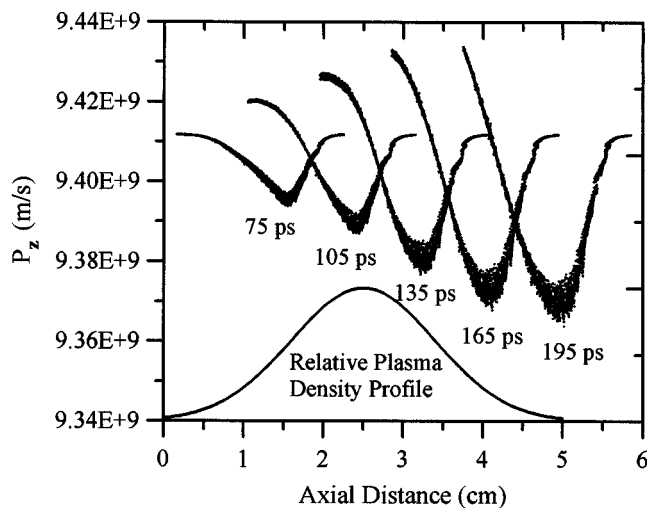


Fig. 10. Electron beam momentum versus axial distance. Here, the momentum is defined by $P_z = \gamma v_z$.

within the beam bunch. However, it should be pointed out that the wake-field effect is quite small and negligible because the energy gain of the tail particles is only 0.2%.

IV. SUMMARY

The thin underdense plasma lens experiment at UCLA was introduced. For the experiment an argon discharge plasma source was developed and tested for various conditions. The test results show that the plasma source can produce appropriate plasma parameters for the designed experiment, i.e., a density of low 10^{12} cm^{-3} and a thickness of a few centimeters. To predict experimental results, simulations with the MAGIC code were performed. For the given parameters, the simulation results show that the beams are dynamically focused with a focal length of about 9 cm, and the beam size (FWHM) is reduced by a factor of 0.38 for $\tau = 2\omega_p^{-1}$ and 0.21 for $\tau = 3\omega_p^{-1}$. For the beam and plasma parameters used for the simulation, a nonlinear focusing effect is evident up to $\tau = 3\omega_p^{-1}$. This kind of nonlinearity can be reduced by using longer beams or higher plasma and beam densities. A longitudinal plasma wake-field effect was investigated in the simulations, but it turned out to be negligibly small.

ACKNOWLEDGMENT

The authors would like to thank G. Hairapetian, who is currently working at Hughes Research Laboratories, for his construction and initial testing of the plasma source.

REFERENCES

- [1] D. Gabor, "A space-charge lens for the focusing of ion beams," *Nature*, vol. 160, no. 4053, pp. 89–90, 1947.
- [2] W. K. H. Panofsky and W. R. Baker, "A focusing device for the external 350-MeV proton beam of the 184-inch cyclotron at Berkeley," *Rev. Sci. Instrum.*, vol. 21, p. 445, 1950.
- [3] P. Chen, "A possible final focusing mechanism for linear colliders," *Part. Accel.*, vol. 20, no. 3–4, pp. 171–182, 1987.
- [4] J. J. Su, T. Katsouleas, J. M. Dawson, and R. Fedele, "Plasma lenses for focusing particle beams," *Phys. Rev. A*, vol. 41, no. 6, pp. 3321–3331, 1990.
- [5] R. Keinigs and M. Jones, "Two-dimensional dynamics of the plasma wakefield accelerator," *Phys. Fluids B*, vol. 30, no. 1, pp. 252–263, 1987.

- [6] M. Pisin Chen, J. M. Dawson, J. M. Robert W, J. M. Huff, and T. Katsouleas, "Acceleration of electrons by the interaction of a bunched electron beam with a plasma," *Phys. Rev. Lett.*, vol. 54, no. 7, pp. 693–696, 1985.
- [7] T. C. Katsouleas, "Physical mechanisms in the plasma wake-field accelerator," *Phys. Rev. A*, vol. 33, no. 3, pp. 2056–2064, 1986.
- [8] J. B. Rosenzweig, P. Schoessow, B. Cole, C. Ho, W. Gai, R. Konecny, S. Mtingwa, J. Norem, M. Rosing, and J. Simpson, "Demonstration of electron beam self-focusing in plasma wake fields," *Phys. Fluids B*, vol. 2, no. 6, pp. 1376–1383, 1990.
- [9] P. Muggli, K. A. Marsh, S. Wang, C. E. Clayton, S. Lee, T. C. Katsouleas, and C. Joshi, "Photo-ionized lithium source for plasma accelerator applications," *IEEE Trans. Plasma Sci.*, vol. 27, pp. 791–799, June 1999.
- [10] H. Nakanishi *et al.*, "Direct observation of plasma-lens effect," *Phys. Rev. Lett.*, vol. 66, no. 14, pp. 1870–1873, 1991.
- [11] G. Hairapetian, P. Davis, C. E. Clayton, C. Joshi, S. C. Hartman, C. Pellegrini, and T. Katsouleas, "Experimental demonstration of dynamic focusing of a relativistic electron bunch by an overdense plasma lens," *Phys. Rev. Lett.*, vol. 72, no. 15, pp. 2403–2406, 1994.
- [12] P. Chen, S. Rajagopalan, and J. Rosenzweig, "Final focusing and enhanced disruption from an underdense plasma lens in a linear collider," *Phys. Rev. D*, vol. 40, no. 3, pp. 923–926, 1989.
- [13] N. Barov and J. B. Rosenzweig, "Propagation of short electron pulses in underdense plasmas," *Phys. Rev. E*, vol. 49, no. 5, pp. 4407–4416, 1994.
- [14] N. Barov, M. E. Conde, W. Gai, and J. B. Rosenzweig, "Propagation of short electron pulses in a plasma channel," *Phys. Rev. Lett.*, vol. 80, no. 1, pp. 81–84, 1998.
- [15] H. Suk, C. E. Clayton, R. Narang, P. Muggli, J. Rosenzweig, C. Pellegrini, and C. Joshi, "Test results of the plasma source for underdense plasma lens experiments at the UCLA Neptune Lab," in *Proc. 8th Workshop Advance Accelerator Concepts*, W. Lawson, C. Bellamy, and D. F. Brosius, Eds. Baltimore, MD, 1998, pp. 501–513.
- [16] B. Goplen, L. Ludeking, D. Smithe, and G. Warren, "User-configurable MAGIC for electromagnetic PIC calculations," *Comput. Phys. Commun.*, vol. 87, pp. 54–86, 1995.
- [17] J. B. Rosenzweig, S. Anderson, K. Bishofberger, X. Ding, A. Murokh, C. Pellegrini, H. Suk, A. Tremaine, C. Clayton, C. Joshi, K. Marsh, and P. Muggli, "The Neptune photoinjector," *Nucl. Instrum. Meth. A*, vol. 410, no. 3, pp. 437–451, 1998.
- [18] P. Davis, "Plasma lenses for relativistic electron beams," Ph. D. dissertation, Dept. Elec. Eng., Univ. California Los Angeles, 1996.
- [19] N. A. Krall and A. W. Trivelpiece, *Principles of Plasma Physics*. San Francisco, CA: San Francisco Press, 1986, ch. 6.10.3.

H. Suk, photograph and biography not available at the time of publication.

C. E. Clayton, photograph and biography not available at the time of publication.

C. Joshi, photograph and biography not available at the time of publication.

T. C. Katsouleas, photograph and biography not available at the time of publication.

P. Muggli, photograph and biography not available at the time of publication.

R. Narang, photograph and biography not available at the time of publication.

C. Pellegrini, photograph and biography not available at the time of publication.

J. B. Rosenzweig, photograph and biography not available at the time of publication.